communications earth & environment

Article

https://doi.org/10.1038/s43247-024-01428-1

Atmospheric destabilization leads to Arctic Ocean winter surface wind intensification

Martina Zapponini & Helge F. Goessling

The surface-amplified winter warming over the Arctic Ocean is accompanied by a pronounced intensification of near-surface winds, simulated by climate models and emerging in reanalysis data. Here, the influences of sea-ice decline, wind changes aloft, and atmospheric stability are revisited based on CMIP6 historical and high-emission scenario and ERA5 reanalysis data. Spatial trend patterns suggest that near-surface wind intensification over the inner Arctic Ocean in winter is largely driven by an increasing downward momentum transfer due to a weakening atmospheric stratification. In contrast, a near-surface wind intensification in summer appears to be largely driven by accelerating winds aloft, amplified in a high-emission future by decreasing surface roughness due to sea-ice decline. In both seasons, differences in near-surface wind-speed trends are closely linked to atmospheric stability trends. Models suggest that by 2100 the lower troposphere may become as unstable in winter as in summer, implying a fundamental regime shift of the Arctic winter boundary layer.

Since 1950, Arctic surface air temperatures have increased at a rate two to four times the planetary average[1–4]. This, observed[2,5,6] and projected[7–9], Arctic amplification owes to feedbacks related to sea ice[5,10–12], temperature[13–15], water vapor and clouds[16,17] as well as remote factors related to poleward heat and moisture transport[14,17,18]. Arctic amplification is most pronounced during winter and close to the surface but largely absent during summer and above 850 hPa (~1.5 km height)[14,19]. This distinct spatio-temporal warming pattern is largely due to the strong stratification of the Arctic lower troposphere associated with temperature inversions during winter and linked with the lapse-rate feedback[13–15]. At the same time, the warming pattern implies that the stratification during winter weakens, and with it, the amplitude of the seasonal cycle of lower-tropospheric stability.

Weaker stratification enables stronger turbulence and thereby enhances vertical mixing of air and the properties it carries. This includes the transfer of horizontal momentum from the free troposphere and upper boundary layer towards the surface, thereby affecting the vertical wind profile[20–22]. The wind profile can feedback on atmospheric stability by affecting turbulence and mixing, in particular in regions of strong stability where wind shear is the primary source of turbulence[23]. This complex interplay is difficult to disentangle, but in any case, a thermally forced destabilization by surface-amplified warming is expected to strengthen the vertical momentum transfer. A strong influence of lower-tropospheric stability on near-surface winds in the lowest portion of the boundary layer, including at the standard observing height of 10m, has long been described for very different parts of the globe. For example, near-surface winds are relatively decoupled from the strong flow aloft above the equatorial Pacific cold tongue[24]. Moreover, a negative relation between stratification and the ratio between surface stress and geostrophic wind has been observed in the Arctic[25,26].

Consistently, in a high-emission scenario, climate models contributing to the Coupled Model Intercomparison Project phase 5 (CMIP5)[27] simulate a pronounced increase in near-surface wind speeds by up to 23% in winter over parts of the Arctic Ocean until the end of the 21st century[28]. This could have major implications for the evolution of sea ice[29–31] and ocean waves[32], and thereby on Arctic marine navigation and coastal erosion[33].

Apart from reduced atmospheric stability, two more causal factors have been discussed, namely reduced surface roughness due to sea-ice decline and changes in atmospheric horizontal temperature and pressure gradients that may influence the storm tracks and wind patterns more generally[12,28,34–39]. It has been suggested that the latter plays a sub-ordinate role, and the relative importance of atmospheric stratification versus surface roughness is still debated[28,39].

The separation of these two factors is challenging because both are strongly affected by sea ice. First, sea ice is typically rougher than the open ocean[26,28,34,35], although the relation between sea-ice concentration, effective roughness, and ocean stress is complex and exhibits a maximum at

Alfred Wegener Institute, Helmholtz Centre for Polar and Marine Research, Bremerhaven, Germany. e-mail: martina.zapponini@awi.de

intermediate sea-ice concentrations[40,41]. Second, sea ice and the snow on top of it hinder warming of the near-surface air by latent cooling and reflection of solar radiation in summer, and by insulating the cold air from the warmer ocean in winter[12]. Correspondingly, strong negative correlations in time and space between sea-ice concentration and near-surface wind speed have been documented[36,42,43], but two recent analyses trying to disentangle the contributions from surface roughness and atmospheric stability remain inconclusive.

One study based on CMIP5 projections concludes that "some combination of weakened atmospheric stability and reduced surface roughness" leads to the strengthening of surface winds[28]. Finding that one pair of similar models exhibits decreasing near-surface wind speeds despite decreasing atmospheric stability, it is argued that "surface roughness may be critical for explaining the sign and magnitude of future wind changes over the marine Arctic"[28]. Another study approaches the separation of these two mechanisms more directly with dedicated sensitivity experiments where the sea-ice surface roughness is modified such that it resembles the smoother open ocean in a coupled climate model[39]. With surface roughness trends thereby removed, it is found that the wind-speed increase until 2100 in a high-emission scenario is reduced over the Arctic Ocean on average by ~40% in autumn but only by ~10% in winter[39]. In contrast, much weaker but still positive near-surface wind-speed trends in spring and summer are turned into slightly negative trends by the elimination of the roughness effect—consistent with the finding that the atmosphere tends to become more stable during these times of the year[39], when the remaining ice keeps the near-surface air temperature close to the freezing point while increasingly warm air is advected aloft from lower latitudes.

Here, changes in Arctic Ocean near-surface winds and their link to sea-ice decline and atmospheric stability are revisited based on ERA5 reanalysis[44,45] as well as historical and high-emission scenario data of the CMIP6[46]. It is shown that a coherent increase in winter near-surface wind speed, absent in reanalysis data over the satellite era since 1979[29,43], emerges in the Central Arctic when data since 1950 are included, despite negligible sea-ice concentration trends. While pre-1979 reanalysis data are more uncertain and trends in reanalyses must be regarded with caution[47], the ERA5 historical trends are consistent with CMIP6 data. A tight relation between stratification trends and wind-speed profile trends across seasons and data sets is demonstrated, suggesting a dominant role of lower tropospheric stability in past and future Arctic wind trends.

Results

Near-surface patterns of trends

According to ERA5, Arctic winter (January, February, March; JFM) 2-meter temperature exhibits an ubiquitous surface warming over the Arctic Ocean (Fig. 1d), with two hot spots in the East Greenland and Barents Seas. These coincide with the areas of highest sea-ice concentration reduction (Fig. 1a). However, a clear near-surface warming trend also prevails beyond these seas, where the sea-ice concentration in winter has not yet declined; averaged over the inner Arctic Ocean (delineated in Fig. 1e and termed Arctic Ocean hereafter), the linear warming trend 1950–2020 is +0.8 K per decade, five times the global average trend exhibited by ERA5 for the same period (Supplementary Fig. 1). The CMIP6 multi-model mean exhibits similar trend patterns over the historical (including 2015–2020 scenario) period (Fig. 1b, e), although only the Barents Sea appears as a hot spot which is spatially more diluted, largely due to model differences in the ice-edge location (Supplementary Figs. 2 and 3); the Arctic Ocean average 2-meter temperature trend is +0.6 K per decade (range [+0.3, +1.3] K per decade; Fig. 2a). The trend steepens in the high-emission scenario and reaches +1.4 K per decade (range [+0.7, +2.6] K per decade) averaged over the extended period 1950–2100 (Fig. 2b). Some sea-ice decline now also reaches the central Arctic (Fig. 1c). The marginal seas still exhibit the strongest sea-ice trends, but they do not appear as warming hot spots anymore relative to the strong warming across the Arctic Ocean (Fig. 1f).

While there is no clear positive trend in near-surface wind speed across the Arctic Ocean in reanalysis data since 1979 (Supplementary Fig. 1; see also refs. 29,43), an ubiquitous speed-up, on average by 1% per decade (0.06 m s^{-1} per decade), emerges when ERA5 data since 1950 are included (Fig. 1g). This is consistent with CMIP6, although the historical CMIP6 mean trend is weaker (0.4% per decade; Fig. 1h). There is substantial model spread, with some models, such as AWI-CM-1-1-MR[48], capturing the amplitude and pattern of the ERA5 wind-speed trend much better than others (Supplementary Fig. 4). The AWI-CM-1-1-MR ensemble exemplifies that the near-surface wind-speed trend pattern is fairly robust among the ensemble members, whereas the historical period seems to be too short to derive reliable trends for wind vectors.

As for the warming, the near-surface wind-speed trend steepens when the whole 21st century is included (1.15% per decade; Fig. 1i). Importantly, the wind-speed trend patterns resemble more closely the near-surface warming than the sea-ice concentration trends, in particular over the historical period (Fig. 1g, h). This provides the first evidence that near-surface warming, through its influence on atmospheric stability, may be more important than the sea-ice concentration decrease per se, through its influence on roughness.

Vertical structure of trends

To elucidate trends in atmospheric stability and vertical momentum transfer further, it is expedient to relate the near-surface trends to those further aloft. Consistent with earlier works[14,19], both ERA5 and CMIP6 model data exhibit about three times faster warming close to the surface compared to the free troposphere, at and above the 850 hPa level, over the Arctic Ocean in winter (Fig. 2a, b). This implies a reduction of the inversion strength (Fig. 2c, d, g, h) and thus a weakening of the atmospheric stratification. The CMIP6 spread is large, but all models exhibit a negative temperature gradient trend that becomes even steeper when including the whole 21st century (Fig. 2d).

At the same time, relative wind speed trends exhibit a local maximum at the surface in ERA5 and in all models for both periods (Fig. 2e, f). This is consistent with enhanced vertical momentum transfer towards the surface, although it could also be caused by reduced surface roughness (further discussed below). Three models with a negative wind speed trend at 850 hPa exhibit a slightly negative trend also at the surface over the historical period, but the remaining 16 models exhibit a positive near-surface trend, consistent with ERA5's winds strengthening by 1% per decade at the surface compared to 0.2% per decade at 850 hPa. Over the extended period, all models simulate increasing near-surface wind speeds, combined with a near-neutral to moderately negative wind speed trend at 850 hPa (Fig. 2f).

The largely negative wind speed trends in the free troposphere may at least partly have the same cause as the near-surface wind acceleration, namely the increased downward momentum transfer. However, the slowdown aloft may also be due partly to a weakening of the Arctic large-scale circulation, possibly in response to the reduced lower-tropospheric meridional temperature gradient. To filter out possible effects from large-scale circulation changes and to isolate the relation between atmospheric stability and momentum transfer, the following analysis relates trends in the temperature difference between the lower free troposphere and the near-surface to trends in the wind-speed ratio between the near-surface and the lower free troposphere, similar as in[43]. The wind speed ratio essentially measures how strongly the near-surface winds are coupled to the free-tropospheric winds. It is influenced, on the one hand, by the efficiency of downward momentum transfer across the whole boundary layer and, on the other hand, by how strongly the near-surface wind is attenuated by near-surface turbulence due to surface roughness. Thus both a weakened thermal stratification and a reduced surface roughness can cause an increased wind-speed ratio, whereas changing free-tropospheric winds, at first order, do not affect the wind-speed ratio.

The top of the Arctic boundary layer is typically a few hundred meters up to one kilometer above the surface[23,36,49]. This implies that the 850 hPa pressure level at ~1.3 km altitude (marked by a gray line in Fig. 2) is just

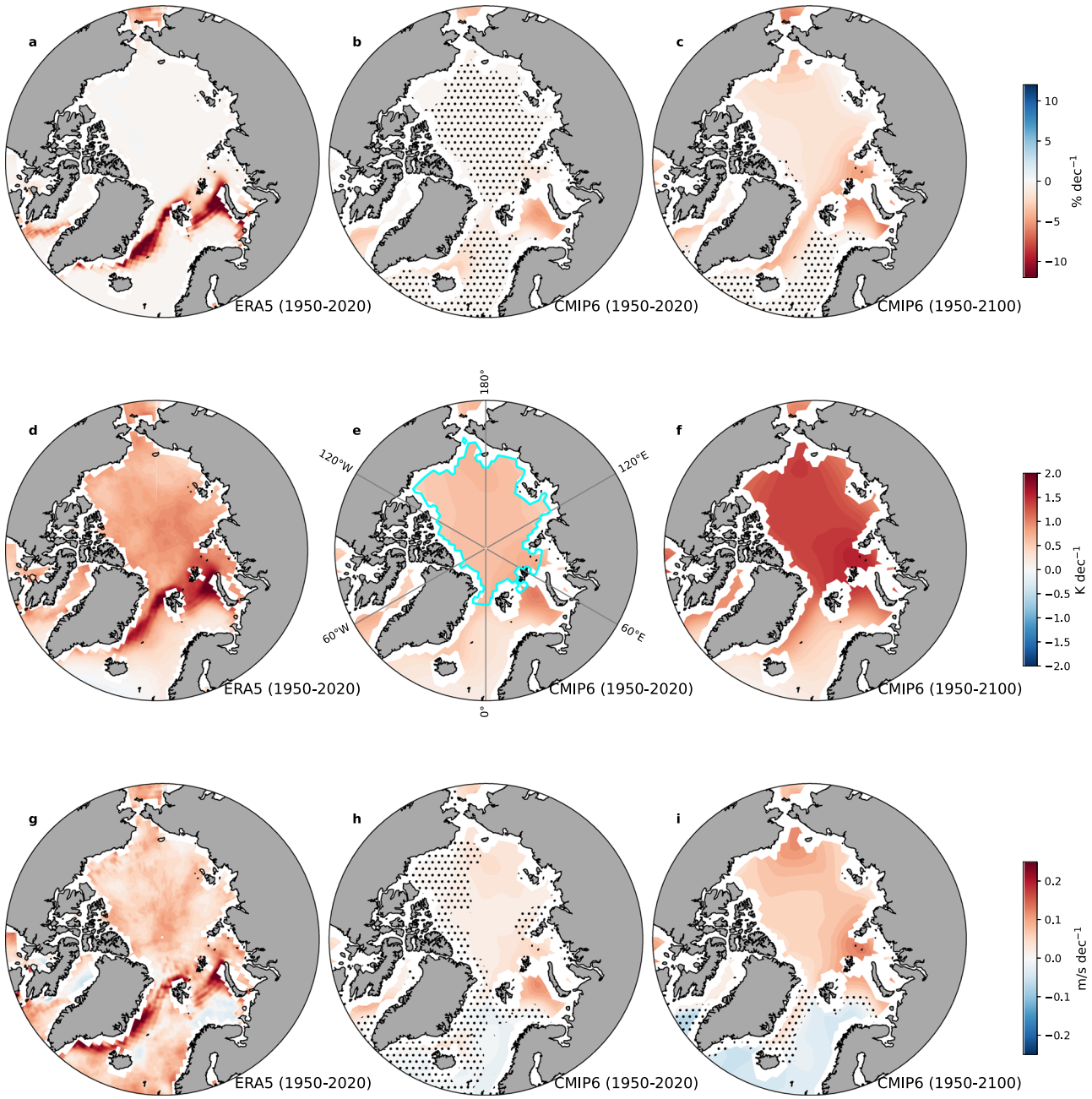

Fig. 1 | Arctic winter (JFM) mean trends in sea-ice concentration, 2-meter temperature, and 10-meter wind speed. Arctic winter mean trends in sea-ice concentration (**a**–**c**), 2-meter temperature (**d**–**f**), and 10-meter wind speed (**g**–**i**). The trends are based on ERA5 and the CMIP6 multi-model mean for the periods 1950–2020 and 1950–2100, as indicated in the bottom right side of each map. The mask for spatial averages is delineated in **e**. Statistical significance of local CMIP6 multi-model mean trends is based on a two-sided one-sample *t* test for difference from zero; stippling indicates non-significant trends ($p > 0.05$).

above the maximum boundary layer height and can be considered representative of the lowest part of the free troposphere. The 850 hPa level, as well as the 10 m wind and 2 m temperature levels, are standard output and thus available from both ERA5 and CMIP6 data, so we use this to derive the wind speed ratio.

Relation between stratification and wind-speed ratio

Model differences regarding trends in stratification and trends in the wind-speed ratio in winter are highly and significantly anti-correlated and proportional, for both the historical ($R = -0.84$, slope -1.1% per K) and the extended ($R = -0.95$, slope -1.5% per K) period (Fig. 3a, b), precisely matching the ERA5 relation in the first case. The winter CMIP6 multi-model mean exhibits a very similar slope of -1.35% per K and an almost exactly linear progression of subsequent decadal means from 1950 to 2100 (Fig. 4b). The weaker inter-model correlation for the shorter historical period (Fig. 3a) as well as the less stringent progression of ERA5 winter decadal means (Fig. 4a) may simply be due to a lower signal-to-noise ratio caused by internal variability. Indeed, the ensemble spread (indicated by the crosses in Fig. 3a, b) of most individual models is about as large as the average signal over the historical period but not over the longer period. The overall tight relation between stratification and wind-speed ratio suggests a dominant role of trends in atmospheric stability for the intensification of Arctic Ocean near-surface winds in winter.

In summer (July, August, September; JAS), the sea-ice, temperature, and wind speed mean states and trends are markedly different (Supplementary Figs. 5 and 6). The warming over the Arctic Ocean is on average

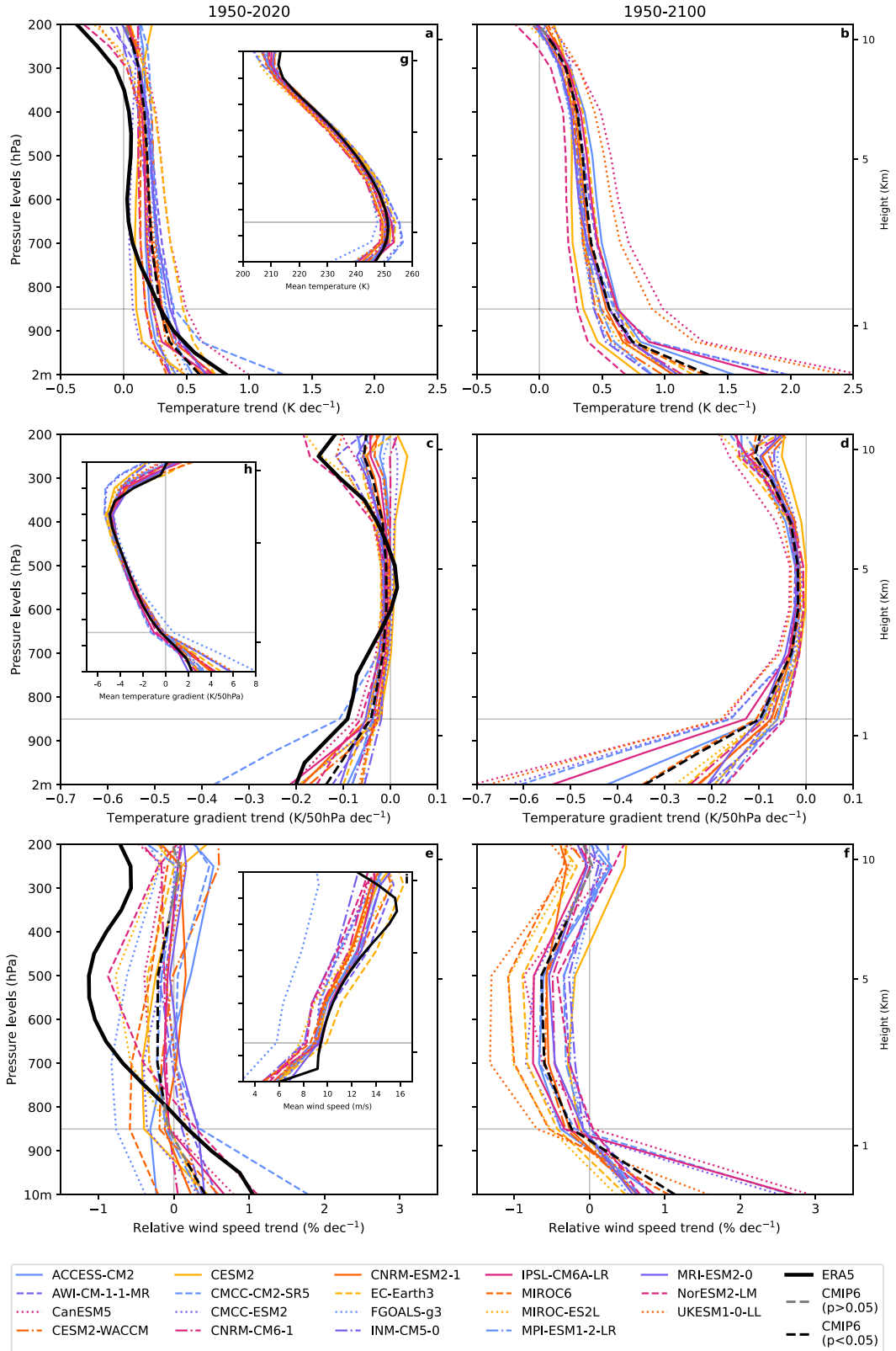

Fig. 2 | Vertical profiles of Arctic Ocean winter (JFM) mean trends in air temperature, vertical temperature gradient, and wind speed. Vertical profiles of Arctic Ocean winter mean trends in air temperature (**a**, **b**), vertical temperature gradient (**c**, **d**), and wind speed (**d**, **e**). The period 1950–2020 (**a**, **c**, **e**) includes both ERA5 (black solid line) and CMIP6 models (colored lines), while the extended period 1950–2100 (**b**, **d**, **f**) includes only CMIP6 models. Insets (**g**–**i**) show the corresponding mean profiles for 1950–2020. The gray horizontal line marks the 850 hPa level at ~1.3 km altitude in the lower free troposphere. Statistical significance of the CMIP6 multi-model mean trend (dashed black/gray curve) is based on a two-sided one-sample *t* test for difference from zero.

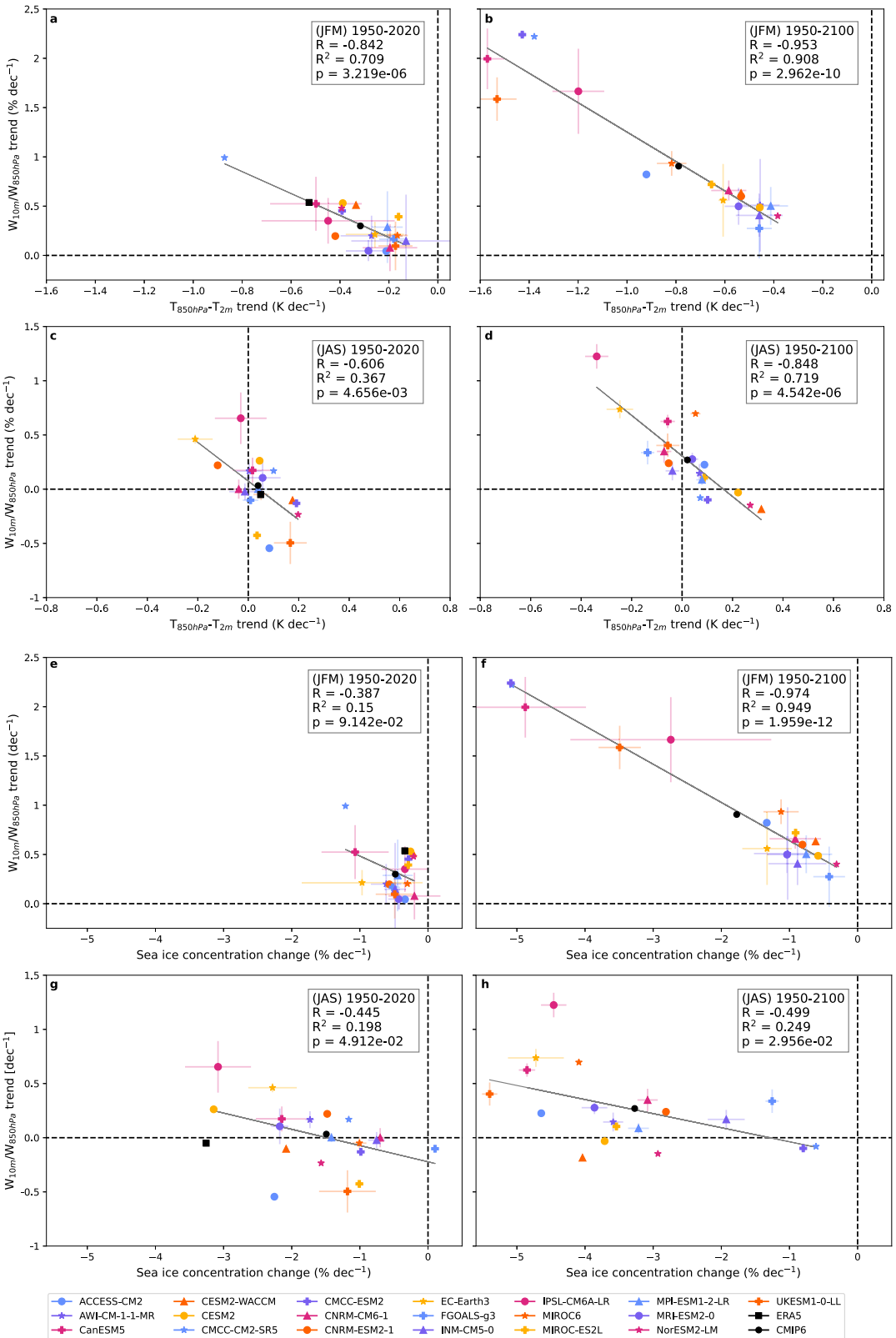

Fig. 3 | Linear trends in wind speed ratio, vertical temperature gradient, and sea ice concentration. Linear trend in wind-speed ratio versus (**a**–**d**) linear trend in temperature difference between near-surface and 850 hPa levels and versus (**e**–**h**) linear trend in sea ice concentration. Winter, JFM, and summer, JAS, seasons are included. The period 1950–2020 includes both ERA5 (black square) and CMIP6 models (colored symbols), while the extended period 1950–2100 includes only CMIP6 models. The black dots show the multi-model mean trends. Lines denote linear least-square fits. For each model with more than one ensemble run included in the study, the ensemble spread is shown.

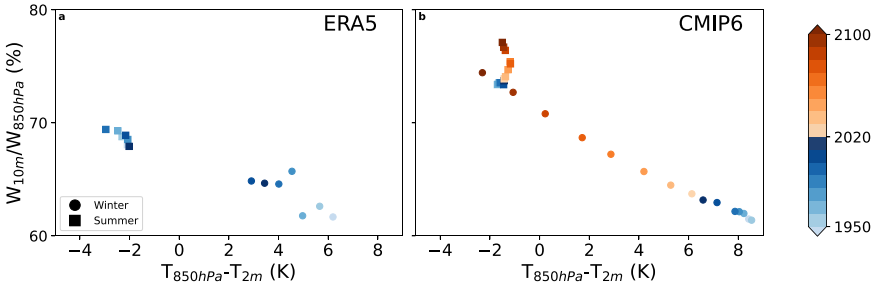

Fig. 4 | Decadal means of wind speed ratio and vertical temperature gradient. Decadal means of wind-speed ratio versus temperature difference between near-surface and 850 hPa levels in winter (JFM, circles) and summer (JAS, squares), for ERA5 1950–2020 (**a**) and the CMIP6 multi-model mean 1950–2100 (**b**).

quite homogeneous throughout the troposphere, although some models simulate a near-surface dampening of the warming and thus a stabilization, consistent with[39], whereas others simulate a near-surface amplification and thus a destabilization of the atmosphere (Supplementary Fig. 6a–d). Consistently, wind-speed ratios are not changing uniformly (Supplementary Fig. 6e, f), but again there is a highly significant anti-correlation ($R = -0.61$, slope −1.8% per K and $R = -0.85$, slope −1.9% per K) between the trend in stratification and the trend in wind-speed ratio (Fig. 3c, d).

ERA5 data exhibit a slight stabilization and decreasing wind-speed ratio in summer so that the summer and winter conditions approach each other in terms of stratification and wind-speed ratio (Fig. 4a), resulting in an attenuated amplitude of the seasonal cycle. Decreasing seasonality occurs also in the CMIP6 multi-model mean (Fig. 4b), but only because of the changes in winter. In summer, the CMIP6 multi-model mean stratification and wind-speed ratio remain unchanged over the historical period, but the wind-speed ratio gradually increases over the course of the high-emission scenario despite constant stratification.

Contributions from sea-ice decline and large-scale winds

Another factor may contribute to the projected increase of the wind-speed ratio over the Arctic Ocean in summer, namely the decreasing surface roughness resulting from the profound sea-ice decline, consistent with[28,39]. While other factors can affect ocean surface roughness, in particular sea state, here we consider only sea-ice concentration. Indeed, 15 out of the 19 models exhibit an area-averaged decrease of the summer sea-ice concentration beyond 40% (−2.67% per decade over 1950–2100), and 12 of these exhibit an increasing wind-speed ratio (Fig. 3h). Given this link, one may ask again more generally which factor is primarily driving the response of the wind-speed ratio: the thermal stratification or the surface roughness?

Relating changes in the wind-speed ratio to changes in sea-ice concentration across CMIP6 models for the long period 1950–2100 in winter reveals that the two are also closely anti-correlated ($R = -0.97$, slope −0.39% per %; Fig. 3f). Given the close link between the surface warming and the sea-ice decline in this case, the high anti-correlation with both sea-ice decline and temperature gradient reduction provides limited evidence to determine which factor is actually driving the response of the wind-speed ratio. More prominent differences arise when considering the situation in summer, where the long-term anti-correlation with the sea-ice concentration trend drops considerably ($R = -0.5$, slope −0.13% per %; Fig. 3h), whereas the anti-correlation with the temperature gradient remains much higher ($R = -0.77$; Fig. 3d). An even stronger contrast is evident for the historical period in both winter and summer (Fig. 3e, g): the correlations with the sea-ice concentration trend is weak and barely statistically significant in winter ($R = -0.39$, slope −0.3% per %) and summer ($R = -0.45$, slope −0.15% per %), in contrast to the medium to high correlations with the temperature gradient trend ($R = -0.84$ and -0.61; Fig. 3a, c). Combined with the better-matching spatial trend patterns (Fig. 1), the more robust link between the vertical temperature gradient and the wind-speed ratio across seasons and periods suggests that changes in the thermal stratification are dominating the response of the wind speed ratio rather than changes in surface roughness.

Finally, the near-surface wind speed trend can be influenced not only by changes in thermal stratification and surface roughness, which affect the wind speed ratio, but also by possible wind-speed changes aloft. The slowdown of the free-tropospheric winds in winter (Fig. 2e, f) can be interpreted as a direct consequence of the increased downward momentum transfer. However, some of the deceleration aloft may also be driven by changes in the large-scale circulation. This could explain why some models simulate only a weak winterly near-surface wind intensification over the extended period despite a pronounced weakening of the atmospheric stratification. In contrast, free-tropospheric summerly wind speeds are increasing in ERA5 and in most models in concert with the near-surface wind intensification (Supplementary Fig. 6e, f). While model differences between the near-surface and free-tropospheric relative wind-speed trends are related to the change in stratification also in summer (Fig. 3c, d), the vertically more homogeneous trends suggest that the increased wind speeds in summer can not be linked to enhanced vertical mixing or decreased surface roughness alone, but that they are mostly due to large-scale drivers.

Discussion

The ERA5 and CMIP6 data analyzed here suggest that the past and future near-surface wind intensification over the inner Arctic Ocean in winter is largely driven by an increasing downward momentum transfer due to a weakening atmospheric stratification, possibly damped by decelerating large-scale winds aloft. In contrast, the near-surface wind intensification in summer is largely driven by accelerating winds aloft, amplified in a high-emission future by decreasing surface roughness due to sea-ice decline. In both seasons, differences in wind-speed ratio trends and, thus, near-surface wind-speed trends between data sets, including models as well as ERA5, are closely linked to differences in atmospheric stability trends.

These results are qualitatively consistent with earlier work[28,39]. However, while we do not quantify the contributions with exact estimates but rather infer them from pattern similarity, the concluded relative importance of the factors contributing to near-surface wind-speed trends over the Arctic Ocean is different. Here, it is concluded that diminishing surface roughness due to sea-ice decline contributes notably only in summer over the course of the next decades, but not over the historical period, and in winter scarcely at all. A high anti-correlation between long-term simulated winter trends in wind-speed ratio and sea-ice concentration seems to be largely due to the close physical link between surface warming and sea-ice decline. Instead, our results suggest that trends in atmospheric stability play a dominant role and also largely explain differences between models. Moreover, large-scale wind-speed trends aloft may modify the near-surface wind speed trends, with a rather decelerating effect in winter and an accelerating effect in summer.

A clear limitation is that the validity of these results depends on the fidelity of the models to simulate the relevant processes. This pertains not only to CMIP6, but also to ERA5 where the polar boundary layers may be among the regions that are least well constrained by observations and thus depend most on the model formulation[50]. Another relevant caveat of ERA5 is that the sea-ice thickness is assumed to be constant, with no snow on top, leading to a surface warm bias in winter[51] and to an inability to represent a contribution to the winter surface warming from sea-ice and snow thinning[52]. Moreover, trends in reanalyzes must be regarded with caution

because they can be affected by discontinuous availability of assimilated observations[47]. Yet, for the same reason that reanalyzes are weakly constrained in the Arctic boundary layer, multi-decadal trends across the inner Arctic Ocean can not be evaluated by actual observations: because these are spatio-temporally too scarce[50].

Bearing this in mind, the CMIP6 simulations suggest that, until the end of this century, in a high-emission scenario, the lower troposphere may become as unstable in winter as it is and remains in summer. The efficiency of downward momentum transfer would align seasonally likewise. This implies a fundamental regime shift of the Arctic winter near-surface winds and boundary layer, more generally, likely with major repercussions on the sea ice and ocean below, affecting ocean waves, marine navigation, and coastal erosion.

Methods

Models and data

All climate model data used here are from the CMIP6 dataset[46,53]. The period 1950–2020, referred to as the historical period here, is composed of the CMIP6 historical simulations (1950–2014) and the first years of the SSP370 scenario simulations (2015–2020); the period 2021—2100 is based on the remainder of the SSP370 scenario simulations. The model selection was determined by the availability of data for the required variables at the required temporal frequency, i.e., daily resolution for wind velocity components and monthly resolution for both air temperature and sea-ice concentration. ERA5 reanalysis data, covering the period 1979–2020[44] and the preliminary backward extension 1950–1978[45], have been used as reference for both air temperature and wind speed fields.

Wind speed is not an archived variable for CMIP6 models, except for the surface level in a few cases. To obtain a consistent dataset, monthly wind speed was computed by averaging daily wind speed derived from daily wind velocity components. Using monthly sampled velocity components, and thus not capturing sub-monthly variations in wind direction and speed, would have implied an underestimation of average wind speeds by about a factor of two[54] and could have distorted the obtained trends.

Apart from 10-meter wind speed, 2-meter air temperature, and sea-ice concentration, slightly different pressure levels have been used for different data sets and variables due to data availability constraints. For CMIP6, 5 pressure levels (850, 700, 500, 250, 100 hPa) have been used for wind and 10 (925, 850, 700, 600, 500, 400, 300, 250, 200 hPa) for air temperature (original pressure levels without interpolation). For ERA5, 19 pressure levels from 950 hPa to 50 hPa, with intervals of 50 hPa, have been used for both variables.

For most of the models, all ensemble members with the required variables available in the aforementioned frequency and for the full time period considered, have been included in the study, see Table 1. For the few models with more than 10 ensemble members only the first 10 have been used. All the Figures showing results for individual models show ensemble means. The only exception is the AWI-CM-1-1-MR model in Supplementary Figs. 2–4, where all five ensemble members are shown individually to exemplify the robustness of the derived trend patterns given internal variability. While the exact magnitude of internal variability varies between data sets, including models as well as reality and how it is captured by ERA5, the same order of magnitude can be expected[55].

Data analysis

Spatial trends (Fig. 1 and Supplementary Fig. 5) are based on the original horizontal grid for ERA5, whereas CMIP6 data have first been remapped to a common 1.25° × 1.85° latitude-longitude grid. Multi-model means have been computed afterwards. From four of the models considered (CESM2-WACCM, CESM2, FGOALS-g3, and NorESM2-LM), only the near-surface wind speed and no velocity components were available on the ESGF platform (see Supplementary Fig. 4). These have been included in the multi-model wind speed mean, but not in the multi-model wind vector field mean. Results for individual models (Figs. 2 and 3 and Supplementary Figs. 2–4, 6) have been derived separately based on the original horizontal model grids.

Table 1 | CMIP6 climate models included in the study

Model	Ensemble runs	Model	Ensemble runs
ACCESS-CM2	3	FGOALS-g3	2
AWI-CM-1-1-MR	5	INM-CM5-0	5
CanESM5	10	IPSL-CM6A-LR	10
CESM2-WACCM	1	MIROC6	3
CESM2	1	MIROC-ES2L	1
CMCC-CM2-SR5	1	MPI-ESM1-2-LR	10
CMCC-ESM2	1	MRI-ESM2-0	5
CNRM-CM6-1	6	NorESM2-LM	1
CNRM-ESM2-1	1	UKESM1-0-LL	8
EC-Earth3	2		

All the models included in the study with the number of ensemble runs considered.

The Arctic Ocean domain used for spatial averages is the area north of 68°N for longitudes east of 103°E and west of 124°W, and the area north of 79°N at all other longitudes (Fig. 1e). Grid points on land or within 150 km from any coastline have been omitted to avoid the influence of land and orography, similarly to[54].

Wind speed trends in Fig. 2 and Supplementary Fig. 6 are relative trends, obtained from division by the mean wind speed of the period 1950–2020 for the same model, height, and season. This normalization enables a more direct interpretation of the wind speed trend profiles regarding the efficiency of vertical momentum transfer. Temperature and temperature gradient trends in the same two figures are absolute trends as it is for all the trends shown in Figs. 1 and Supplementary Fig. 5.

Two-sided one-sample t tests have been used to test if CMIP6 multi-model mean trends are significantly different from zero. In Fig. 2 and Supplementary Fig. 6, the results of the t tests are displayed by coloring the multi-model mean curve either black ($p < 0.05$) or gray ($p \geq 0.05$); here, the test has been applied to the area-averaged trends for each pressure level separately. In Fig. 1 and Supplementary Fig. 5, in the CMIP6 mean panels, grid points where $p \geq 0.05$ have been stippled; here, the test has been applied locally for each grid point after performing the remapping.

Data availability

The CMIP6 data are openly available from the Earth System Grid Federation (ESGF, https://esgf.llnl.gov/); they have been, in this case, retrieved from the German Climate Computing Center's (DKRZ) node of the ESGF. The wind velocity components data for the levels above the surface from the historical experiment of AWI-CM-1-1-MR, not available through the ESGF, are archived at the German Climate Computing Center (DKRZ) and are available upon request. ERA5 data are produced by the Copernicus Climate Change Service (C3S) at ECMWF and are openly available on the Climate Data Store (CDS, https://cds.climate.copernicus.eu/). The data and the Jupyter notebooks or Python scripts to reproduce the Figures included in this study are available in the Github repository https://github.com/mzapponi/Arctic_Winds_Intensification_paper.

Received: 26 October 2023; Accepted: 30 April 2024;
Published online: 17 May 2024

References

1. Trenberth, K. et al. Observations: surface and atmospheric climate change. *In:* Solomon, S. et al. (eds.) Climate Change 2007: The Physical Science Basis. Contribution of Working Group 1 to the 4th Assessment Report of the Intergovernmental Panel on Climate Change (Cambridge University Press, 2007).

2. Serreze, M., Barrett, A., Stroeve, J., Kindig, D. & Holland, M. The emergence of surface-based arctic amplification. *Cryosphere* **3**, 11–19 (2009).
3. Arctic Monitoring Assessment Programme (AMAP), N., Oslo. Snow, water, ice and permafrost in the arctic (swipa), 269 pp (2017).
4. Rantanen, M. et al. The arctic has warmed nearly four times faster than the globe since 1979. *Commun. Earth. Environ.* **3**, 168 (2022).
5. Screen, J. & Simmonds, I. Increasing fall-winter energy loss from the arctic ocean and its role in arctic temperature amplification. *Geophys. Res. Lett*. **37** https://doi.org/10.1029/2010GL044136 (2010).
6. Cohen, J. et al. Recent arctic amplification and extreme mid-latitude weather. *Nat. Geosci.* **7**, 627–637 (2014).
7. Stroeve, J. et al. Trends in arctic sea ice extent from cmip5, cmip3 and observations. *Geophys. Res. Lett.* **39**, L16502 (2012).
8. Barnes, E. & Polvani, L. Cmip5 projections of arctic amplification, of the north american/north atlantic circulation, and of their relationship. *J. Clim.* **28**, 5254–5271 (2015).
9. Shu, Q. et al. Arctic ocean amplification in a warming climate in cmip6 models. *Sci. Adv.* **8**, eabn9755 (2022).
10. Serreze, M. & Barry, R. Processes and impacts of arctic amplification: a research synthesis. *Glob. Planet. Change* **77**, 85–96 (2011).
11. Rampal, P., Weiss, J., Dubois, C. & Campin, J.-M. Ipcc climate models do not capture arctic sea ice drift acceleration: Consequences in terms of projected sea ice thinning and decline. *J. Geophys. Res.: Oceans* **116** https://doi.org/10.1029/2011JC007110 (2011).
12. Vihma, T. Effects of arctic sea ice decline on weather and climate: a review. *Surv. Geophys.* **35**, 1175–1214 (2014).
13. Bintanja, R., Graversen, R. & Hazeleger, W. Arctic winter warming amplified by the thermal inversion and consequent low infrared cooling to space. *Nat. Geosci.* **4**, 758–761 (2011).
14. Pithan, F. & Mauritsen, T. Arctic amplification dominated by temperature feedbacks in contemporary climate models. *Nat. Geosci.* **7**, 181–184 (2014).
15. Feldl, N., Po-Chedley, S., Singh, H., Hay, S. & Kushner, P. Sea ice and atmospheric circulation shape the high-latitude lapse rate feedback. *npj Clim. Atmos. Science* **3**, 1–9 (2020).
16. Vavrus, S. The impact of cloud feedbacks on arctic climate under greenhouse forcing. *J. Clim.* **17**, 603–615 (2004).
17. Taylor, P. et al. A decomposition of feedback contributions to polar warming amplification. *J. Clim.* **26**, 7023–7043 (2013).
18. Previdi, M., Smith, K. & Polvani, L. Arctic amplification of climate change: a review of underlying mechanisms. *Environ. Res. Lett.* **16**, 093003 (2021).
19. Screen, J., Deser, C., Simmonds, I. & Tomas, R. Atmospheric impacts of arctic sea-ice loss, 1979–2009: separating forced change from atmospheric internal variability. *Clim. Dyn.* **43**, 333–344 (2014).
20. Monin, A. & Obukhov, A. Basic laws of turbulent mixing in the surface layer of the atmosphere. *Contrib. Geophys. Inst. Acad. Sci. USSR* **151**, e187 (1954).
21. Louis, J. A parametric model of vertical eddy fluxes in the atmosphere. *Bound.-Layer Meteorol.* **17**, 187–202 (1979).
22. Young, J. Static stability. *Encyclopedia of Atmospheric Sciences*. 2nd edn, **2**, 423–430 (2014).
23. Brooks, I. et al. The turbulent structure of the arctic summer boundary layer during the arctic summer cloud-ocean study. *J. Geophys. Res. Atmos.* **122**, 9685–9704 (2017).
24. Wallace, J. M., Mitchell, T. & Deser, C. The influence of sea-surface temperature on surface wind in the eastern equatorial pacific: Seasonal and interannual variability. *J. Clim.* **2**, 1492–1499 (1989).
25. Brown, R. Modeling the geostrophic drag coefficient for aidjex. *J. Geophys. Res.: Oceans* **86**, 1989–1994 (1981).
26. Overland, J. Atmospheric boundary layer structure and drag coefficients over sea ice. *J. Geophys. Res.: Oceans* **90**, 9029–9049 (1985).
27. Taylor, K. E., Stouffer, R. J. & Meehl, G. A. An overview of cmip5 and the experiment design. *Bull. Am. Meteorol. Soc.* **93**, 485–498 (2012).
28. Vavrus, S. & Alkama, R. Future trends of arctic surface wind speeds and their relationship with sea ice in cmip5 climate model simulations. *Clim. Dyn.* **59**, 1833–1848 (2022).
29. Spreen, G., Kwok, R. & Menemenlis, D. Trends in arctic sea ice drift and role of wind forcing: 1992–2009. *Geophys. Res. Lett.* **38** https://doi.org/10.1029/2011GL048970 (2011).
30. Zhang, J., Lindsay, R., Schweiger, A. & Steele, M. The impact of an intense summer cyclone on 2012 arctic sea ice retreat. *Geophys. Res. Lett.* **40**, 720–726 (2013).
31. Yu, X. et al. Evaluation of arctic sea ice drift and its dependency on near-surface wind and sea ice conditions in the coupled regional climate model hirham–naosim. *Cryosphere* **14**, 1727–1746 (2020).
32. Dobrynin, M., Murawsky, J. & Yang, S. Evolution of the global wind wave climate in cmip5 experiments. *Geophys. Res. Lett.* **39** https://doi.org/10.1029/2012GL052843 (2012).
33. Overeem, I. et al. Sea ice loss enhances wave action at the arctic coast. *Geophys. Res. Lett.* **38** https://doi.org/10.1029/2011GL048681 (2011).
34. Knippertz, P., Ulbrich, U. & Speth, P. Changing cyclones and surface wind speeds over the north atlantic and europe in a transient ghg experiment. *Clim. Res.* **15**, 109–122 (2000).
35. Wadhams, P. Ice in the Ocean (Gordon and Breach Science Publishers, 2000).
36. Seo, H. & Yang, J. Dynamical response of the arctic atmospheric boundary layer process to uncertainties in sea-ice concentration. *J. Geophys. Res. Atmos.* **118**, 12–383 (2013).
37. Mioduszewski, J., Vavrus, S. & Wang, M. Diminishing arctic sea ice promotes stronger surface winds. *J. Clim.* **31**, 8101–8119 (2018).
38. Alkama, R. et al. Wind amplifies the polar sea ice retreat. *Environ. Res. Lett.* **15**, 124022 (2020).
39. DuVivier, A. et al. Investigating future arctic sea ice loss and near-surface wind speed changes related to surface roughness using the community earth system model. *J. Geophys. Res. Atmos.* **128**, e2023JD038824 (2023).
40. Lüpkes, C., Gryanik, V., Hartmann, J. & Andreas, E. A parametrization, based on sea ice morphology, of the neutral atmospheric drag coefficients for weather prediction and climate models. *J. Geophys. Res. Atmos.* **117** https://doi.org/10.1029/2012JD017630 (2012).
41. Martin, T., Steele, M. & Zhang, J. Seasonality and long-term trend of arctic ocean surface stress in a model. *J. Geophys. Res.: Oceans* **119**, 1723–1738 (2014).
42. Zhang, J., Stegall, S. & Zhang, X. Wind–sea surface temperature–sea ice relationship in the chukchi–beaufort seas during autumn. *Environ. Res. Lett.* **13**, 034008 (2018).
43. Jakobson, L., Vihma, T. & Jakobson, E. Relationships between sea ice concentration and wind speed over the arctic ocean during 1979–2015. *J. Clim.* **32**, 7783–7796 (2019).
44. Hersbach, H. et al. The era5 global reanalysis. *Q. J. R. Meteorol. Soc.* **146**, 1999–2049 (2020).
45. Bell, B. et al. The era5 global reanalysis: preliminary extension to 1950. *Q. J. R. Meteorol. Soc.* **147**, 4186–4227 (2021).
46. Eyring, V. et al. Overview of the coupled model intercomparison project phase 6 (cmip6) experimental design and organization. *Geosci. Model Dev.* **9**, 1937–1958 (2016).
47. Swart, N., Fyfe, J., Gillett, N. & Marshall, G. Comparing trends in the southern annular mode and surface westerly jet. *J. Clim.* **28**, 8840–8859 (2015).
48. Semmler, T. et al. Simulations for cmip6 with the awi climate model awi-cm-1-1. *J. Adv. Model. Earth Syst.* **12**, e2019MS002009 (2020).
49. Peng, S. et al. The characteristics of atmospheric boundary layer height over the arctic ocean during mosaic. *Atmos. Chem. Phys.* **23**, 8683–8703 (2023).

50. Jung, T. et al. Advancing polar prediction capabilities on daily to seasonal time scales. *Bull. Am. Meteorol. Soc.* **97**, 1631–1647 (2016).
51. Batrak, Y. & Müller, M. On the warm bias in atmospheric reanalyses induced by the missing snow over arctic sea-ice. *Nat. Commun.* **10**, 4170 (2019).
52. Landrum, L. & Holland, M. Influences of changing sea ice and snow thicknesses on simulated arctic winter heat fluxes. *Cryosphere* **16**, 1483–1495 (2022).
53. O'Neill, B. et al. The scenario model intercomparison project (scenariomip) for cmip6. *Geosci. Model Dev.* **9**, 3461–3482 (2016).
54. Tandon, N., Kushner, P., Docquier, D., Wettstein, J. & Li, C. Reassessing sea ice drift and its relationship to long-term arctic sea ice loss in coupled climate models. *J. Geophys. Res. Oceans* **123**, 4338–4359 (2018).
55. Cheung, A. et al. Comparison of low-frequency internal climate variability in cmip5 models and observations. *J. Clim.* **30**, 4763–4776 (2017).

Acknowledgements

We acknowledge the CMIP community for providing the climate model data, globally distributed in the framework of the ESGF. The CMIP data of this study were mirrored and made available for this study by the DKRZ. All the analyses were performed at the German Climate Computing Center (DKRZ), in the framework of the project ab0995, on the Levante supercomputer. We acknowledge the financial support by the Federal Ministry of Education and Research of Germany in the framework of SSIP (grant 01LN1701A). The authors extend their gratitude to Dr. Gianluca Redaelli and Dr. Lorenzo Sangelantoni for their suggestions and useful discussions during the preliminary analyses of the study.

Author contributions

H.F.G. designed the study, M.Z. retrieved and processed the data. Both authors contributed to the writing and reviewing of the manuscript.

Funding

Open Access funding enabled and organized by Projekt DEAL. We acknowledge support by the Open Access Publication Funds of Alfred-Wegener-Institut Helmholtz-Zentrum für Polar- und Meeresforschung.

Competing interests

The authors declare no competing interests.

Additional information

Supplementary information The online version contains supplementary material available at https://doi.org/10.1038/s43247-024-01428-1.

Correspondence and requests for materials should be addressed to Martina Zapponini.

Peer review information *Communications Earth & Environment* thanks the anonymous reviewers for their contribution to the peer review of this work. Primary Handling Editors: Mengze Li, Heike Langenberg. A peer review file is available